ASSESSING LAND USE AND LAND COVER CHANGE IMPACT ON FLASH FLOODS IN KASARANI CONSTITUENCY, KENYA

Japheth Ominde*

*University of Debrecen, Department of Geography and Geoinformation Systems.

*Corresponding Author: -

Abstract

Kasarani Constituency in Nairobi County, Kenya is one of the areas that experienced frequent flash floods over the last decade. Anthropogenic activities such as the construction of roads, buildings, and industrialization are identified as key drivers of change in LULC. The aim of this study was to assess the impact of LULC change on flooding in the Kasarani constituency by comparing Spectral indices from Landsat images captured before, during, and after floods between 2013 and 2020. The value of NDVI and MSAVI indices declined during flood days indicating that the vegetation was covered with water while the NDMI value increased during flood days indicating a water-logged surface. The Digital Elevation Model of the study area was created to identify the low-lying areas and river channels that were identified as high flood risk areas. In order to reduce vulnerability to frequent floods, there is a need to identify safe areas for evacuation as well as raised areas for settlement.

Key Words: *Land use, Land cover, Spectral Indices, Floods, Remote Sensing.*

TABLE OF CONTENTS

INTRODUCTION

There has been a sharp increase in not only the magnitude, but also the frequency of hydrological hazards particularly flash floods in the immediate past which has been linked to climate change, and alterations stemming from land use, cover and management (Dammalage & Jayasinghe, 2019). The flash floods that are as a result of surface runoff in urban settings are amongst the most dangerous natural hazards producing the greatest damage to human communities. Whereas floods may occur naturally due to intensifying rainfall or heavy rainfall over a short period, anthropogenic activities have been identified as key drivers of incessant floods, especially in urban settings (Guzha et al., 2018). Intense anthropogenic activities like industrialization, building, and road construction have been catapulted by the high demand created by the growing human population in urban environs and the burden of having to meet human wants such as shelter, food, transport, and sanitation among others (Abuya, 2020). In the process of utilizing the land to acquire human wants, profound effects on somehow pristine land are introduced over time. The most significant ones are patterns in land use and land cover (LULC) (Hussein et al., 2020). Consequently, LULC change decreases natural open zones but permits the growth of impervious surfaces, such as rooftops, driveways, parking lots, and roads which in turn contribute to abundance in not only streamflow but also runoff volume. Concomitantly, that heightens levels of peak discharge, all of which lead to degradation of the hydrology of a watershed. The comprehension of hydrological processes' effects that are linked to changes in LULC is critical for policymakers to adopt sustainable plans for water and land recourses management.

Barnsley and Barr (2020) define land cover as tangible or physical materials found on land's surface which include grass, concrete, tarmac, and water. Land use on the other hand is regarded as the human activity that takes place on or makes

use of land for residential, commercial, or industrial activity (Barnsley & Barr, 2020). Many studies on patterns of LULC reveal that changes in LULC have taken place to threatening proportions (Mundia, 2017). The situation has made LULC change to be one of the critical environmental concerns that the global society seeks to address (Acha & Aishetu, 2018). LULC is instrumental in the maintenance of atmospheric energy and its alteration poses significant risks to human livelihoods (Guhza et al., 2018). This is in tandem with the Intergovernmental Panel on Climate Change (IPCC) 2021 report that details the effects of alterations in LULC on climate change. The report ranks flooding at the top of frequent natural disasters and devastating global effects which include property damage, loss of lives, displacement of people, and social disruption.

In Kenya, high incidences of floods were experienced in the periods 1961-1962 and 1997-1998, with the latter being associated with the El Nino occurrence (Masese et al., 2016). In the last twenty years, floods that cause massive damage and loss of lives in Kenya have had a recurring pattern (Okaka & Odhiambo, 2018). According to the Emergency Events Database (EM-DAT) report of 2020, out of the 6 flood incidences that were reported in Kenya between 2010 and 2020, five of those incidences affected Nairobi County with damages ranging from the displacement of people, loss of property, and the destruction of infrastructures such as schools, roads, and water reservoirs.

The Kasarani constituency is an electoral constituency in Kenya. According to KNBS (2019), Kasarani tops the list in terms of population density in Nairobi City County. Consequently, this area, in which the study is conducted, has an ever-growing demand for housing and owning a home. Most low-lying parts that were considered hassocks and water absorbers have increasingly been converted into built-up lands. Surprisingly, because of poor land regulations by the county government, land merchants have sub-divided plots in dimensions of 50m x 50m (0.25 hectares) to fetch more profits from real estate developers and those seeking places to construct homes. Notably, the small portions of land in this area are neither controlled nor planned. The partitioning of the small parcels of land within the study area is uncontrolled and unplanned (Mwathi, 2016). Besides the buildings, unplanned landscaping of frontages and massive corridor network constructions such as the Thika superhighway, eastern by-pass, and residential connections have been installed thereby contributing to conurbation. The growing infrastructure has introduced impregnable surfaces which contribute to increased surface run-off and reduced percolation. These surface changes stir the growth of inundation areas as well as the frequency of floods, thereby posing a livelihood safety challenge to the occupants and commuters in these environs.

Further, to engineer flood management and mitigation strategies, it is worthwhile to assess the status of the surface especially before, during, and after flood events. Luckily the remote sensing and geographic information system (GIS) has made it possible to acquire and integrate data from different sources and dates to assess the trends in surface characteristics, quantify change, and identify the type and the place of change (Ejikeme et al., 2020). Essentially, information extracted from spectral images is used to study the changes in vegetation cover over time. This study aims to assess the impact of LULC change on flooding in the Kasarani constituency by; 1. Comparing three Spectral indices from Landsat images captured before, during, and after flooding. 2. Statistical observation of the Spectral indices. 3. Observing the Digital Elevation model of the study area.

2. LITERATURE REVIEW

2.1. Landsat program

The Landsat initiative involves earth-observing satellite mission series that is managed by the United States Geological Survey (USGS) and the National Aeronautics and Space Administration (NASA). The first satellite launched by the NASA-USGS partnership in 1972 was known as Earth Resources Technology Satellite (ERTS-1). This was later named Landsat-1. Since then, other Landsat satellites (Landsat 2-9) illustrated in Table1 were set up to capture and store remote sensing data of the world, thus creating a rich and continuous heritage of Landsat archives with a wide range of utilization (Hemati et al., 2021). For instance, the over 50-decade Landsat archive was employed as a source of reference for scientific, economic, and government-related projects, generating useful information on land-use changes for environmental policymakers and fostering partnership at both local and international levels (Zhu et al., 2019; Hemati et al., 2021).

Each Landsat satellite has a specific sensor that is mounted to acquire data in different frequency ranges of the electromagnetic spectrum. The Landsat-1 satellite had a Return Beam Vidicon (RBV) to collect data for cartographic applications, and Multispectral Scanner System (MSS) with 60 meters spatial resolution, and a 6-bit quantization system that collected data in four bands. Whereas RBV data was used in cartography, the MSS was designed to collect spectral data for analyzing terrestrial features (Lauer et al., 1997). Landsat-2 and Landsat-3 commissioned in 1975 and 1978 respectively also had MSS and RBV sensors, but they were designed to realize a whole global coverage and capture periodic images (Hemati et al., 2021). In addition to MSS, the Thematic Mapper (TM) onboard Landsat-4 and 5 which were put to use for the first time in 1982 and 1984 respectively, had an 8-bit quantization system and collected data in 7 bands. The TM sensor-enabled capturing of data in thermal and shortwave infrared bands in addition to those found in previous satellites. Concerning Landsat-6 which was engineered in 1993, the Enhanced Thematic Mapper (ETM) sensor mounted on it did not have data collection success since it crushed before achieving any orbit (Lauer et al., 1997). Fortunately, Landsat-5 which had an extended lifetime than expected covered the duration previously intended for the Landsat-6. For Landsat-7, Enhanced Thematic Mapper Plus (ETM+) sensor captured data in the panchromatic band in addition to those found in earlier sensors. In early 2013, Landsat-8 containing Operational Land Imager (OLI) and the Thermal Infrared Sensor (TIRS) were launched. Although it had the same 30 meters spatial resolution which resembles the previous Landsat satellites, its quantization was improved to 12-bit and the number of bands was increased to 11

(Hemati et al., 2021). The recently launched Landsat-9 satellite with a higher quantization of 14-bits has a very similar Operation Land Imager-2 (OLI-2) sensor aboard as OLI of Landsat-8 and an improved version of Thermal Infrared Sensor-2 (TIRS-2). The improved TIRS-2 was designed to rectify the problem of scene select mirror and stray light incursion incidences which occurred in TIRS (Lulla et al., 2021).

Table 1: Landsat Satellites and Sensors

Satellite	Launch date	Sensors
Landsat-1	23rd July 1972	MSS and RBV
Landsat-2	22nd January 1975	MSS and RBV
Landsat-3	5th March 1978	MSS and RBV
Landsat-4	16th July 1982	TM and MSS
Landsat-5	1st March 1984	TM and MSS
Landsat-6	5th October 1993	ETM
Landsat-7	15th April 1999	ETM+
Landsat-8	11th February 2013	OLI and TIRS
Landsat-9	27th September 2021	OLI-2 and TIRS-2

From the time it was engineered, Landsat satellites provide the longest and uninterrupted time series of remotely sensed data (Wulder et al., 2019). These data continue to be used effectively by researchers to detect changes in the earth's surface and resource monitoring. The introduction of free access to the Landsat archive in 2008 led to the development of new data processing approaches, innovation, and understanding era (Dwyer et al., 2018). This period was further fortified by the introduction of Landsat 8, which adds to the archive a high number of daily acquisitions with better geolocation precision and radiometric properties. For instance, Wulder et al. (2019) envision that since the 2013 launch of improved Landsat 8, the total number of images captured and Landsat 8 specific downloads from the USGS archive are about half a million and over 1 million respectively. The high demand for already processed data to save time by scientists, especially in studies related to terrestrial global change led to advancements in data delivery. This was achieved through the reprocessing of all Landsat 1 to 8 archives, resulting in the production of ready-to-use Collection-1 data from 2017 (Dwyer et al., 2018). The provision of data with harmonious radiometric and geometrically corrected surface reflectance makes users direct more time on analysis rather than preprocessing for analysis.

The second major reprocessing effort of the Landsat archive was marked by the introduction of Landsat Collection-2, which contains analysis-ready data products. The Collection-2 Landsat products contain Level-1 data from all sensors since 1972 and global Level-2 surface reflectance and temperature scene-based products since 1982. The Collection-2 Level-2 products are more reconcilable with other earth observation platforms. Meanwhile, Level-2 products are generated from Collection-2 Level-1 inputs that meet the <76 degrees Solar Zenith Angle constraint and include the required auxiliary data inputs to generate a scientifically viable product (Internet 1).

2.2. Spectral Indices

The development of remote sensing and GIS has generated new methods of analyzing satellite imagery with a lot of ease. Passive remote sensing instruments detect and capture electromagnetic energy that is reflected by the sun in various wavelengths (bands). These captured radiations from the Earth's surface constitute multi-temporal and multi-spectral images that can be utilized in the management of surface vegetation and other natural resources (Olmos-Trujillo et al., 2020). For instance, multi-temporal and multi-spectral Landsat imageries have widely been used in studies about forest resources, water quality, pollution, mapping, and vegetation (Sakai et al., 2015; Cui et al., 2013; Olmos-Trujillo et al., 2020). Spectral indices are known to be band ratios that are used in the determination of a particular type of land cover. The use of spectral indices has gained prominence due to its ability to detect specific land covers, ability to compensate for background effects and correct atmospheric distortions, and allow evaluation of the ecosystem (Olmos-Trujillo et al., 2020). There are many spectral indices used by the remote sensing community in monitoring land cover resources such as soil, water, and vegetation (Cui et al., 2013). For this study, Normalized Difference Vegetation Index (NDVI), Normalized Difference Moisture Index (NDMI), and Modified Soil Adjusted Vegetation Index (MSAVI) are used.

The NDVI constitutes the normalized value of the difference in reflectance between near-infrared and red-bands and has mostly been used to characterize changes in vegetated surfaces (Mishra & Mainali, 2017). It is computed using the Equation (Tucker, 1979) below.

$$\mathbf{NDVI} = \frac{\mathbf{NIR - R}}{\mathbf{NIR + R}}$$

where NIR is the near-infrared band, and R is the red band. The NDVI values range between -1 and +1 where negative values indicate water, bare soils, and snow and higher values indicate dense vegetation (Tucker, 1979).

The vegetation characterization while utilizing NDVI is aided by its ability to follow climatic trends such as precipitation (Emmett et al., 2019). This relation between NDVI and precipitation is further enhanced by existing site-specific conditions like topography, LULC, and the type of soil (Mishra & Mainali, 2017). Based on this relationship between

NDVI and precipitation and compounding factors, Wanyama et al. (2020) conducted a study on the impact of natural and human activities on persistent trends in vegetation greening and browning in Mount Elgon Ecosystem, Kenya. In this study, Moderate-resolution Imaging Spectrometer (MODIS) NDVI and precipitation data between 1986 and 2018 were utilized. NDVI and precipitation composites for different periods were created and used in the generation of mean NDVI. Results indicated that greening and browning which were significantly affected by the change in precipitation occurred during the planting season at varying rates in the southwestern part of Mt. Elgon, especially where deforestation had taken place.

The MSAVI is mostly used where the surface is characterized by bare soil or low vegetation cover. It is designed to be a substitute especially when NDVI provides invalid data due to low vegetation or low chlorophyll in the vegetation. MSAVI is computed using the equation (Qi et al., 1994) below;

$$\mathbf{MSAVI} = \mathbf{2 * NIR + 1} - \frac{\sqrt{(\mathbf{2 * NIR + 1})^2 - 8\,(\mathbf{NIR - R})}}{\mathbf{2}}$$

The MSAVI values range between -1 and +1 where lower values indicate the absence of vegetation, while higher values indicate dense vegetation. Olmos-Trujillo et al. (2020) carried out a study to find out the responses of vegetation indices to Spatio-temporal changes in rainfall and temperature in a semi-arid region. The study applied remote sensing and GIS technologies to analyze the trend of MSAVI and other vegetation indices in each season of the year between 2014 and 2018. Results of the analysis showed that vegetation indices varied across the four seasons. However, extremely low MSAVI values were observed when rainfall intensified and exceeded 200mm per month.

The NDMI is used to determine soil moisture content. It is calculated as a ratio between NIR and short-wave infrared band (SWIR) (Vermote et al., 2016).

$$\mathbf{NDMI} = \frac{\mathbf{NIR - SWIR}}{\mathbf{NIR + SWIR}}$$

The NDMI values range between -1 and +1, where high values indicate flooded and water-logged areas while low values indicate dry soils (Vermote et al., 2016).

NDMI is mostly used to detect water-logged and flooded areas, especially in low-lying areas where the slope variation is almost negligible, thereby encouraging water accumulation and stagnation. According to Li (2012), water-logged conditions are partly created by human activities such as the haphazard construction of roadways, buildings, and built-up areas. The built-up landscape, therefore, creates an impervious surface that inhibits the infiltration and percolation of rainwater, leading to variations in soil moisture in different seasons of the year. Based on this school of thought, Sahu and Bengal, (2018) used NDMI and other vegetation indices to detect water-logged areas in Panskura-Tamluk floodplain in India. Further, to detect variations in soil moisture Landsat imageries captured during the floods of November 2013, before floods in March 2013, and after floods in April 2014 were utilized. The NDMI values range before, during, and after floods were 0.770-0.888, 0.814-0.942, and 0.782-0.920 respectively. Results of the analysis indicated that high values of NDMI were recorded during the November rain season which caused floods in the Panskura-Tamluk flood plain.

2.3. Impact Of LULC Change On Flooding

LULC changes reflect the behavior of the human race, with great influence on flooding and its associated problems such as damage to property, loss of lives, and population displacement (Brody et al., 2011). This implies that a clear understanding of LULC changes and the associated impacts on flooding can help local authorities to develop a land-use plan that reduces vulnerability and increase resilience to flood impacts. The evolution of impervious surfaces in built areas from open green spaces and farmlands alters erosional and hydrological characteristics thereby increasing inundations (Lee & Brody, 2018). Through the lenses of Dammalage and Jayasinghe (2019), the conversion of open spaces, agricultural lands, and grasslands in the suburbs of the Colombo district into other uses occasioned increased area under floods between the flood incidence of 1989 and of May 2016. The study utilized Landsat images to identify land use by using NDVI, Normalized Difference Water Index (NDWI), and Normalized Difference Built-up Index (NDBI) indices. A sharp increase in a built-up area and a reduction in green and agricultural areas were observed. It is reported that shrunk open spaces, poor waste disposal, and clandestine constructions impeded water infiltration, and necessitated high floods even though the rainfall amount received was lower in May 2016 compared to 1989.

Moreover, Acha and Aishetu (2018) conducted a study on "Spatio-temporal changes of LULC dynamics and its implication on urban flood vulnerability in Makurdi, Nigeria". In the study, GIS and remote sensing technologies were used to detect LULC change from 1986, through 2006 and 2016. A digital elevation model with classes ranging from high to low flood risk areas was created and soil infiltration analysis was conducted in various sections of the study area. Findings on soil infiltration capacity revealed a low infiltration rate in places of high soil density of 1.46 grams and moisture content of 89%, thereby being identified as flood risk areas. The built-up area extended into floodplains between 1986 and 2016 by 4.82% and 35.36% respectively. From the analysis Land use patterns, low altitude, and expansion of built-up areas are instrumental causes of incessant floods in the area.

Furthermore, Idowu and Zhou (2021) assessed the impact of LULC change in the context of flood hazards in Lagos between the years 1986 and 2020. A map-matrix-based, post-classification LULC change detection method was used to estimate the change in land cover for the study period. The mainland cover types mapped were water, wetland, vegetation, and developed lands. The results indicated a 69% decrease in wetlands and a 94% increase in the developed area during

the study period. It was also noted that while wetland was the dominant land cover type in 1986, in 2020 it covered the smallest extent. The results indicated a strong link between LULC changes and the rise in incessant flooding in Lagos.

In a study covering the Oshiwara river basin in Mumbai India, Zope et al. (2016) used satellite images and topographic maps to estimate land-use change between 1966, 2001, and 2009. The LULC classes used in the study were open land, vegetation, water body, and built-up land. The findings of LULC change analysis revealed a decrease of 42.80% in open spaces, 62% in water bodies, and an increase of 74.84% in built-up areas during the period under study. The impact of these LULC changes on flooding for various return periods was determined using HEC-HMS and HEC-GeoHMS models. A marginal increase in the runoff peak and volume in comparison to the change in LULC. This marginal increase is attributed to a high level of water table which makes the ground to be highly saturated. The high saturation level, therefore, lowers the infiltration rate during the higher return periods for LULC change (Zope et al., 2015). From the analysis, the inundation area increased by 5.61% and 6.04% for 100 and 10-years return periods between the same eras. These findings indicate that LULC change exerts a ripple effect on flood events. If the long-term impacts of LULC change are not factored in while making decisions on individual or government construction projects, more severe floods are likely to occur.

For a long time, Nairobi County continues to experience a change in LULC. The change is noted by Oyugi et al. (2017) in a study conducted to determine the dynamics in LULC and their implications on the environmental quality of Nairobi City between 1988 and 2015. In the study, Landsat TM of 1988 and 1995, Landsat ETM+ of 2000, 2005, 2010, and 2015 images were used. In addition, secondary data such as population between 1988 and 2015, and the city's topographical maps were utilized. The study established that there was a steady growth in built-up areas, especially in the eastern parts of Nairobi between the years 2010 and 2015 as shown in Figures 1. and 2. Similar results were reported by Mundia (2017), a situation that lowers the porosity of the surface, thus triggering floods.
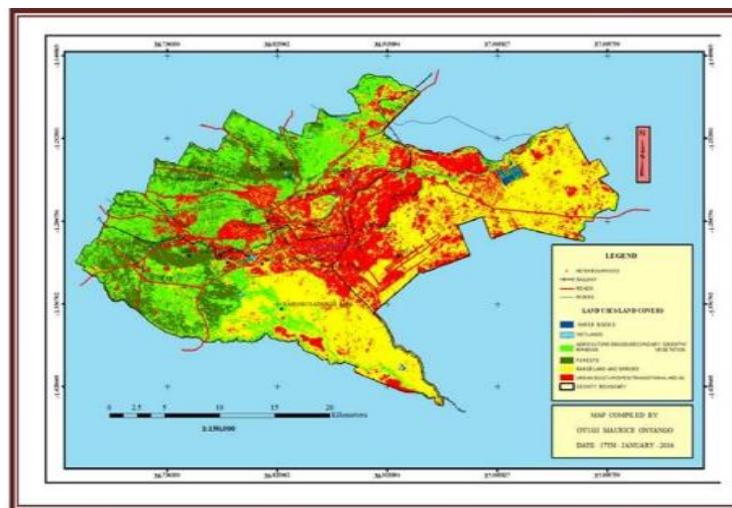

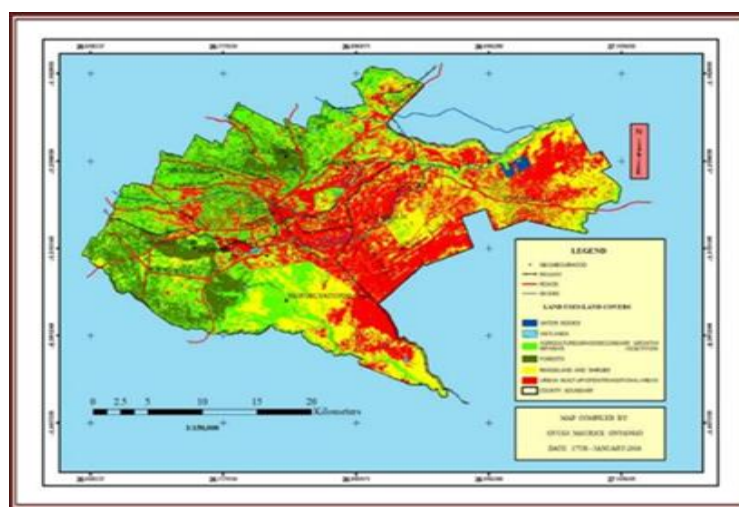**Figure 1**. Nairobi's Built-up area in 2010. Source: Oyugi et al. (2017).

Figure 2. Nairobi's built-up area in 2015. Source: Oyugi et al. (2017).

2.4. Major Development Projects In The Study Area

In recent times, anthropogenic factors in urban areas have become massive with less regard to natural land cover thereby resulting in furious flood incidences. This argument relates to the findings of studies conducted by Guzha et al. (2018) that human activities are the main amplifiers of LULC change which in turn influence the frequent floods in many cities.

Specifically, population increase and its associated pressure on housing, transport, commercial and industrial activities are reported to have accelerated change in LULC in Nairobi County (Oyugi et al., 2017; Mundia, 2017; Mwathi, 2006). Other than population growth and socio-economic factors, Mwathi (2016) appraises land-use decisions as a third key driver of LULC change in the Nairobi metropolitan area. Land use decisions consist of regulations as well as the capacity of institutions mandated in the planning and management of development projects. Since Kasarani is located in Nairobi County, its development projects have been captured in two key recent development projects, that is the Nairobi Metropolitan Development Plan (NMDP) of 2008 and the Nairobi Integrated Urban Development Master Plan (NIUPLAN). These development project plans emanated from the need to create a sustainable city by solving problems caused by rapid population growth and urban sprawl (Mwathi, 2016). The NIUPLAN aim was to provide a framework to guide the management of development projects of Nairobi County from 2014 to 2030, thereby integrating the county development plan with Kenya's Vision 2030. With this development plan, significant levels of achievements especially in infrastructure development such as urban transport, sewer systems, and solid waste management have been realized (Mundia, 2017).

The increase of built-up areas in Nairobi County follows both concentric and sector models of urban growth. Growth in urban areas emanates from the Central Business District (CBD) and nodes of roads that run from the city center which to a large extent does not follow established development master plans (Muthusi et al., 2020). The lack of adherence to existing urban plans has led to the expansion of unplanned built-up areas by the private sector which has had great implications on LULC. Some of the projects within the Kasarani constituency which have been established between 2010 and 2020 under the NMDP and NIULAN include the eastern by-pass (a section of the bi-polar system) shown in Figure 3., sewer treatment plant, Kangundo road renovation, non-motorized walkways, bus stop lay-bys and real estate growth.
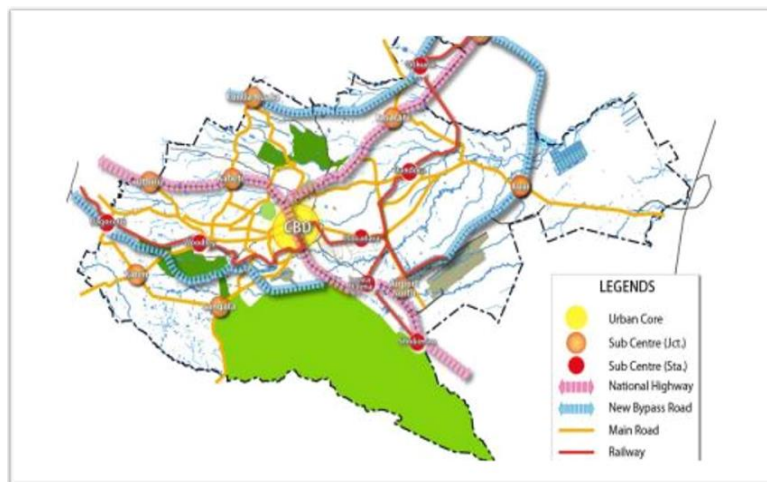

Figure 3. Bypass and node constructions in Nairobi County.
Source: Muema and Officer, (2016).

In the census report of 2009, Nairobi County recorded a total population of about 3.14 million people. This figure rose to about 4.4 million in the 2019 census, which translates to a 40% increase in population between 2009 and 2019 (KNBS, 2019). From the 4.4 million, the Kasarani constituency recorded a total of 780,656 people, making it the second-most populous constituency in Nairobi. According to Mundia (2017), the rapid increase in population exerts strain on existing infrastructures such as housing, transport, water, and sewer systems. Mundia attributes the demand for these services and the local authority's development projects as the main cause of LULC change in Nairobi County. It is also noted that the acute shortage of housing coupled with the need for affordable housing has pushed many low and middle-income earners to settle in areas that were initially unsettled such as Ruai, Kamulu, and their environs.

The settlement attraction in the eastern parts of Nairobi has led to a rise in built-up areas. Specifically, the Kasarani constituency stands out as one of the most sought-after areas by real estate developers such as Fanaka real estate, Kamulu Heights, and Denver Group (Internet 2). With these investors, parts of the Kasarani constituency such as Kamulu and its neighborhoods are ranked among the fastest real-estate areas that continuously experience rapid construction boom without a clearly defined development plan (Mwathi, 2016). Some of the constructions that have been done in the area include commercial centers and new towns, petrol stations, palatial homes, residential roads, supermarkets, recreational joints, hardware shops, and real estate offices. In addition, the availability of huge parcels of land, the newly completed Eastern Bypass, and the well renovated Kangundo road that links Kasarani with Nairobi CBD are the key factors attracting many settlers and real estate companies. Many city dwellers especially those in the middle-class category have established their own homes in the areas such as Ruai and Kamulu, while others have preferred renting from real estate owners (Internet 2).

3. METHODS AND MATERIALS

3.1. Study Area

Figure 4. shows the Kasarani constituency which is one of the constituencies in Nairobi City County of Kenya. With an area of about 135.33km^2, the constituency is located between latitudes 1.2060^{0}S and 1.3042^{0}S and longitudes 36.8850^{0}E and 37.1050^{0}E. It borders Embakasi East, Embakasi North, Ruaraka, Embakasi Central, and Ruaka constituency to the South, Roysambu to the west, Ruiru to the north, and Kangundo constituency to the east. Its distance northeast of Nairobi's central business district is about 16 kilometers. It's bounded by the Thika superhighway. It is divided into five wards that are Clay city, Njiru, Ruai, Mwiki, and Kasarani.

It has a low land terrain with the lowest point being 1455 meters above sea level. The area is drained by river Mathari and Nairobi River which collects its water from river Ngong. The dominant rocks are the phonolytic trachytes that are mainly overlain by Upper Athi Series (UAS). These rocks are mainly composed of sandy sediments, tuffs, thin traces of clay, and intercalated layers of non-porphyritic basalt rocks.
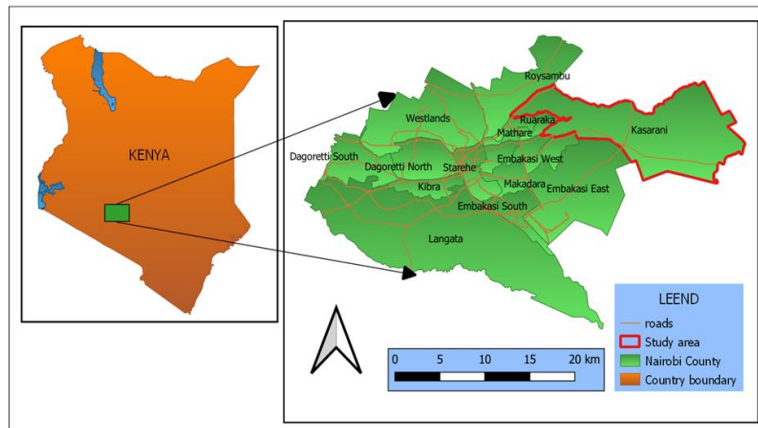

Figure 4. Map of the study area

Regarding climatic conditions, the Kasarani constituency experiences bimodal rainfall where a high rainfall season is received in March, April, and May (MAM), and low rains in October, November, and December (OND) as shown in Table 2. The average annual precipitation is 869mm.

Table 2. Average annual climatic data (Source. (Internet 5))

	Jan	Feb	Mar	Apr	May	Jun	Jul	Aug	Sep	Oct	Nov	Dec
Av. Temp (^{0}C)	19.7	20.2	20.7	20.2	19.1	17.8	16.7	17.2	18.6	19.8	19.3	19.2
Rainfall(mm)	46	48	92	191	144	36	14	19	21	50	128	80

Generally, the Kasarani constituency (part of Nairobi County) experiences a warm temperate climate. March is the warmest month and July the coldest with temperatures of 20.7 degrees Celsius and 16.7 degrees Celsius respectively. Both rainfall and temperature over the study area are mainly influenced by the ITCZ movement (Okoola, 1996). The annual graphical representation of the average climate data is shown in Figure 5.
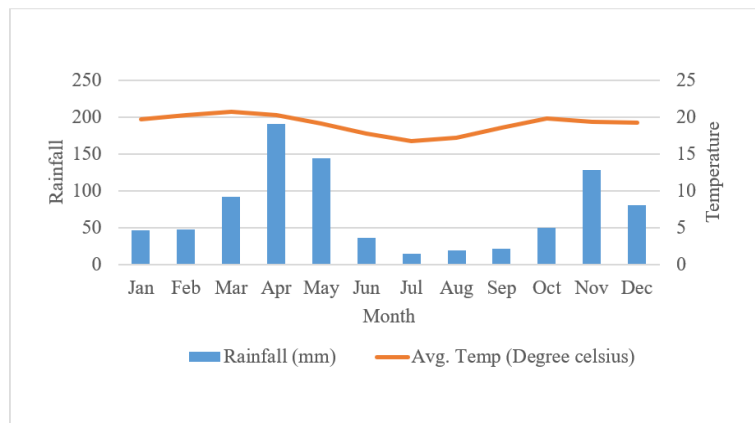

Figure 5. The average annual climate of Nairobi County.

Since the establishment of Nairobi as the Kenya-Uganda railway terminus in 1899, Mundia and Aniya (2006) observed that a significant rise in urban built-up areas is attributed to population and economic growth. The study area has

increasingly become a congested urban society with a total population of 780,656 (KNBS, 2019). To add to that, the study area is a highly residential area with the majority of people running small businesses, while some engage in urban farming and formal employment.

Kasarani constituency is home to Kasarani international stadium, United States International University campuses, technical and vocational training colleges, and international hotels such as Safari Park hotel. The area also has a magnificent shopping complex known as Thika road mall which is located along the Thika superhighway. Other than these already existing infrastructures, topographical factors and the availability of affordable land make the area stand out as one of the most sought-after areas by real estate developers, a situation that has led to urban sprawl. With these investors, parts of the Kasarani constituency such as Kamulu and its neighborhoods are ranked among the fastest real-estate areas that continuously experience a rapid construction boom. Some of the constructions that have been done in the area include commercial centers and new towns, petrol stations, palatial homes, residential roads, supermarkets, recreational joints, hardware shops, and real estate offices. In addition, the availability of huge parcels of land, the newly completed Eastern Bypass and well renovated Kangundo road that connects parts of Kasarani with Nairobi CBD are the key factors attracting many settlers and real estate companies. Many city dwellers especially those in the middle-class category have established their own homes in the areas such as Ruai and Kamulu, while others have preferred renting from real estate owners.

3.2. Data Collection

Landsat data for the days when devastating floods were experienced were collected from the USGS database, from the following periods: 1/3/2010-14/5/2010, 13/1/2013-17/1/2013, 27/4/2015-2/5/2015, 29/4/2016-2/5/2016, 14/3/2018-20/3/2018 and 18/4/2020-1/6/2020 as captured in the Emergency Events Database (EM-DAT). The Landsat images used in this study were of Collection 2, Level-2 which are part of the on-demand surface reflectance products of the Landsat archive. These surface reflectance products of the Level-2 category are both radiometrically and atmospherically corrected (Aljahdali et al., 2021). In this case, Landsat-7 Enhanced Thematic Mapper Plus (ETM+) and Landsat-8 Operational Land Imager (OLI), and Thematic Infrared Sensor (TIRS) imageries with low cloud cover were considered. Path/Row 168/061 on World Reference System (WRS-2) was used in Earth Explorer to determine the region of study.

To process on-demand Level-2 Landsat data, auxiliary input data generated from an external USGS source must be provided. In this case, the product Identifier (IDs) of images for the selected dates were copied in a text file and later used to order Landsat imageries from the USGS Earth Resources Observation and Science (EROS) Center Science Processing Architecture (Internet 3). The text file containing the ID of Landsat scenes was uploaded as an input product in the USGS archive. Additional processing of Level-2 Landsat products selected were spectral indices NDVI, MSAVI, and NDMI. The output products were customized in Geo Tiff, projected to Universal Transverse Mercator (UTM) Zone 37 South coordinate reference system, and resampled using the nearest neighbor method. The submitted order was processed and packaged with components that are specific to Collection2 Level-2 products, and downloaded from the USGS ordering site on 22nd December 2021.

Other shapefile datasets for the boundaries of the study area were downloaded from the global administrative management (GADM) website (Internet 4). GADM database consists of boundary layers of countries and other smaller divisions within a country such as a county, constituency, and ward boundaries. Climate data showing annual average rainfall and temperature patterns extracted from open sources (Internet 5) were also utilized. Shuttle Radar Topography Mission (SRTM) digital elevation model (DEM) was used to generate drainage features and topography of the study area. The summary of the collected data is shown in Table 3.

Table 3. Collected data for the study.

Data	Source	Format	Remarks
Study area shapefiles	GADM website	Shapefile	Undefined
Digital Elevation Model	SRTM downloader	TIFF	30m resolution
Climate data	Climate data.org	Excel/Shapefile	Average temperature and rainfall
Landsat imageries	USGS Website	TIFF	30m resolution
Flood incidence	Emergency Events Database (EM-DAT)	Excel	Days and places affected by floods

3.3. Analysis

Analysis of all Landsat images was carried out in QGIS 3.14 software. In the pre-processing stage, all Landsat images were unzipped before they were loaded in QGIS. The images were already corrected and therefore, no additional radiometric and atmospheric corrections were applied. The images contained surface reflectance products for the study (NDVI, NDMI, and MSAVI). With these indices, the mean, median, and standard deviations were extracted from the study area using the Zonal Statistics tool in QGIS software with the following settings: (1) Adding raster layers containing

spectral indices before, during, and after floods. (2) Clipping raster layers using the study area polygon in the vector layer containing zones section. (3) Selecting mean, median, and standard deviation for processing. The generated values were copied and saved in excel for further analysis. In order to rescale the indices to the desired domain of -1 to +1, the values were multiplied by 0.0001. The mean, median, and standard deviation values were generated for the entire study period. Vegetation index analysis is one of the widely used pre-classification approaches for detecting changes in vegetation cover and its accompanying effects on the environment. The principle behind the pre-classification method where index differentiation is applied is that LULC change causes variation in values of pixel reflectance between the dates of interest (Dewan & Yamaguchi, 2009). A comparative analysis of differences in NDMI, NDVI, and MSAVI mean values in each flood period was carried out to assist in detecting temporal changes in the spectral indices before, during, and after floods. In the case of NDVI and MSAVI, a decrease in index value during floods followed by an increase after floods portended the presence of floodwater on the surface. This is attributed to lower NIR reflection by the spongy mesophyll layer and absorption of the red band by chlorophyll during flood days. In order to detect abrupt changes on the surface due to floods, the mean values were compared. For any positive difference in mean indices between the periods before and during floods, that was interpreted as a flooded surface, while negative differences indicated a retreat of floodwater. In NDMI an increase in value indicated a flooded area while a decrease indicated retreat of floodwater.

The standard deviation and the mean of indices for each flood event were compared. This was done by calculating the difference between standard deviations before and during floods, followed by the difference in value between during and after floods. Statistically, a smaller standard deviation implies that the distribution of indices is clustered around the mean, while high standard deviations mean that the data is more spread out. A reduction in standard deviation was interpreted as clustering of data around the mean implying a similarity in reflectance due to flood water.

The boundary data from GADM was first unzipped and re-projected to UTM (WGS 84 Zone 37S) before it was used for mapping. To assess the impact of LULC change on flooding in the Kasarani constituency, a digital elevation model was needed to provide topographical information such as the flow of rivers and areas that could hold water for longer times after a downpour. Meanwhile, SRTM DEM was used to generate the topography of the study area. The SRTM DEM comprised of two raster tiles covering the study area. The two tiles were merged to form one tile to generate a single DEM. The merged image was clipped and re-projected to UTMWGS 84 Zone 37S. The DEM was then used to generate the slope map which would guide in identifying whether the study area is a low or high-risk flood area. The DEM was further used to generate river networks by first loading the SRTM DEM in QGIS software. The terrain analysis tool was then used to generate Strahler order. A higher-order Strahler of 6 and 4 were used to generate stream channels for Nairobi County and Kasarani constituency respectively. A channel network tool was thereafter used to generate river networks in shapefile format. The river network shapefile was finally clipped to the study area extent and utilized in mapping. The flow chart for research analysis is shown in Figure 6.
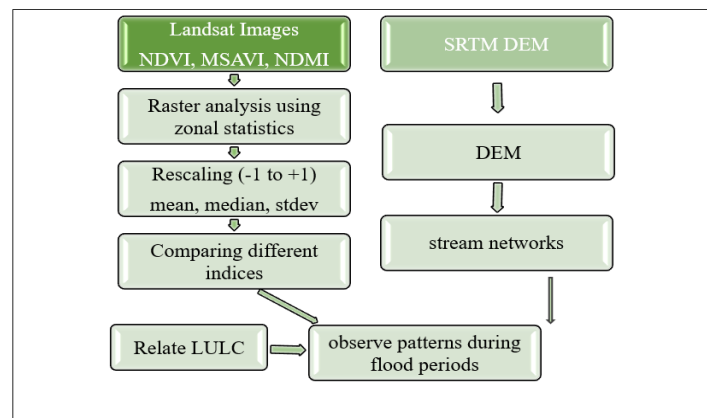

Figure 6: Analysis flow chart.

4.   RESULTS
4.1.   Observing Spectral Indices

The mean values of NDVI, MSAVI, and NDMI derived from Landsat imageries captured before, during, and after flood incidence are shown in Table 4. These indices were generated to help in assessing the condition of the surface during flood periods due to changes in LULC.

Table 4. Mean, Median, and Standard deviation values of Spectral Indices

DAYS	NDMI			NDVI			MSAVI		
	mean	median	stdev	mean	median	stdev	mean	median	stdev
20121222	-0.0048	-0.0207	0.12948	0.27784	0.2848	0.18356	0.13526	0.1321	0.14831
20130224	-0.111	-0.15	0.12997	0.25294	0.2248	0.08874	0.1381	0.1234	0.05706
20130608	0.05768	0.0428	0.12754	0.47547	0.4781	0.12651	0.27137	0.27	0.08863
20150105	-0.0891	-0.1206	0.12407	0.34882	0.3301	0.09942	0.1759	0.165	0.06454
20150427	0.51155	0.5093	0.03324	-0.0055	-0.0057	0.0048	-0.0065	-0.0067	0.00565
20150614	0.07223	0.0468	0.11683	0.51146	0.5113	0.12597	0.27709	0.2718	0.09009
20160225	0.02369	0.0003	0.14593	0.44227	0.433	0.14168	0.24606	0.2368	0.09389
20160429	0.08685	0.0773	0.10907	0.41384	0.4583	0.29017	0.21457	0.2107	0.11708
20160515	0.09998	0.0812	0.11812	0.54062	0.5667	0.17003	0.28899	0.292	0.11652
20180113	-0.0389	-0.0583	0.10002	0.33869	0.3235	0.10055	0.17681	0.1693	0.06166
20180318	0.06001	0.0507	0.0786	0.36461	0.3484	0.09761	0.18015	0.1744	0.05262
20180419	0.16801	0.1568	0.12695	0.52294	0.5658	0.22329	0.27315	0.2589	0.13707
20200220	0.105	0.099	0.12406	0.53364	0.5598	0.15521	0.30281	0.3109	0.11102
20200526	0.09073	0.0734	0.09918	0.43095	0.4794	0.23347	0.23472	0.2175	0.12985
20200611	0.23705	0.2397	0.10038	0.45279	0.4722	0.17069	0.06418	0.047	0.10219
				Flood Days					

Figure 7. (Results): show that NDVI had higher mean values in comparison to MSAVI mean values. However, both NDVI and MSAVI showed a similar trend across the flood periods. The low MSAVI values in comparison to NDVI are due to the ability of MSAVI to discriminate vegetation from background characteristics.
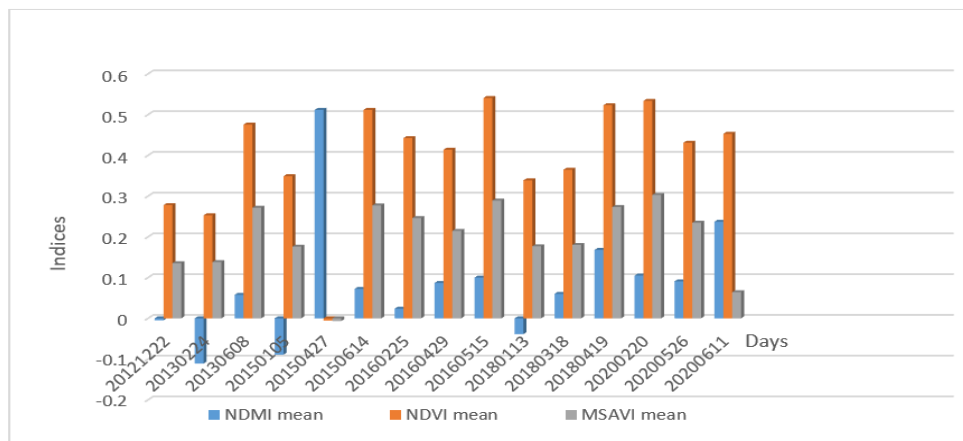

Figure 7. Mean values of spectral indices

In NDMI, an increase in the value of indices indicated flooding while a decrease in value indicated floodwater retreat. Between 2013 and 2020, an increase in the value of NDMI was observed in the floods of 2015, 2016, and 2018. Similar trends were also recorded in the median values of NDVI. In 2015, the changes in the mean value of NDMI before, during, and after floods were -0.0891, 0.5116, and 0.0722 respectively. From the 2015 values, observations are that a sharp increase in NDMI was observed during floods in comparison to the periods when there were no floods.

In the analysis of NDVI, the presence of floodwater was defined by lower mean and median values of indices during flood days in comparison to before and after flood days. In 2013 the mean value before floods was 0.27784, during floods was 0.25294 and after floods, it rose to 0.47547. In 2015, the values before, during, and after floods were 0.34882, -0.0055, and 0.51146 respectively. In 2016 the mean values before, during, and after were 0.44227, 0.41384, and 0.54062 respectively; in 2018 mean values were 0.33869, 0.36461, and 0.52294 for the day before, during, and after floods and 0.53364, 0.43095 and 0.45279 for the 2020 floods as well. From here, it is observed that other than 2018, the period before the floods had a higher NDVI mean value than the flood day value. On the other hand, higher values of NDVI in comparison with flood days were observed after floods across all the years as shown in Figure 8.
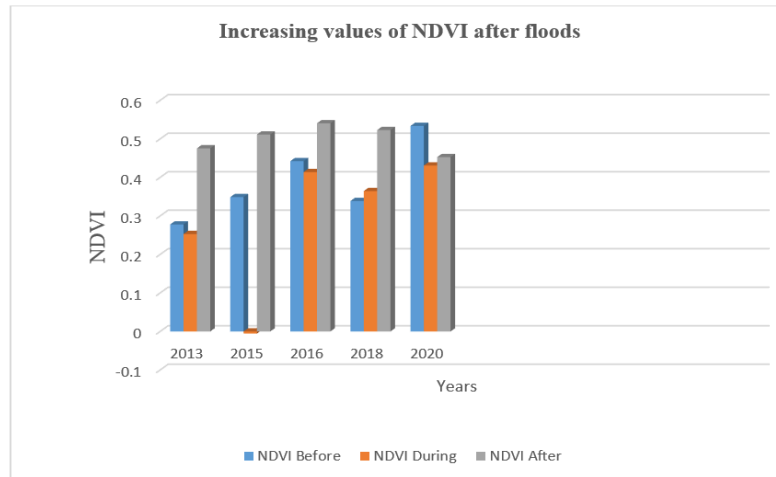
Figure 8. Change of NDVI before, during, and after floods

The low mean values during flood days created two maximum values (taller bars) before and after floods. For instance, in 2013, the mean NDVI before and after floods were 0.2778 and 0.4755 respectively. The low mean values during floods show a decline in NDVI which coincides with the flooding period. Also, the decline in value during flooding was followed by a sharp increase in NDVI after floodwater had subsided. In 2015, two maximum values of NDVI were also observed which relate to days before and after floods. The high values of NDVI before floods were proceeded by a sharp decline that coincided with flood days. A similar pattern is observed in 2016, and 2020 floods. In 2018, the mean value before floods was slightly lower than during floods, but rose abruptly after the flood period, thereby maintaining a similar trend to other years after flood incidence. A similar trend in MSAVI was observed.

Further analysis of results in Table 5. was done to relate huge changes in mean values with LULC change between 2013 and 2020. In this case, the highest difference in mean values during floods (decline by 0.35432) and after floods (increase by 0.517) was recorded in 2015. Similarly, in 2020 a high decline in mean value was observed during flood day. In all the after-flood days, a huge increase in NDVI and MSAVI indices was observed in 2013, 2015, 2016, and 2018.

Table 5. The difference in mean values of spectral indices during and after floods

YEAR	NDVI		MSAVI		NDMI	
	During	After	During	After	During	After
2013	0.0249	-0.2225	-0.0028	-0.1333	0.10614	-0.1687
2015	0.35432	-0.517	0.18243	-0.2836	-0.6006	0.43932
2016	0.02844	-0.1268	0.03148	-0.0744	-0.0632	-0.0131
2018	-0.0259	-0.1583	-0.0033	-0.093	-0.0989	-0.108
2020	0.10268	-0.0218	0.0681	0.17054	0.01427	-0.1463

Figure 9. shows the results of further analysis on NDVI, MSAVI, and NDMI, where the median and mean values of spectral indices before, during, and after floods were also compared. In this case, the difference between the mean and median value of indices of each period was calculated. The results from the comparison in Figure 9. showed a changing pattern in NDVI. It was observed that apart from 2013, the difference between the mean and median values was low on days when floods occurred in comparison to days with no floods. At the same time, the difference in values was also found to be negative on most of the days with and without floods. Statistically, a smaller mean than the median indicates a negative skewness and vice versa. All the three indices showed a declining trend in the difference between the mean and median values with a sharper declining trend being observed in NDVI values.
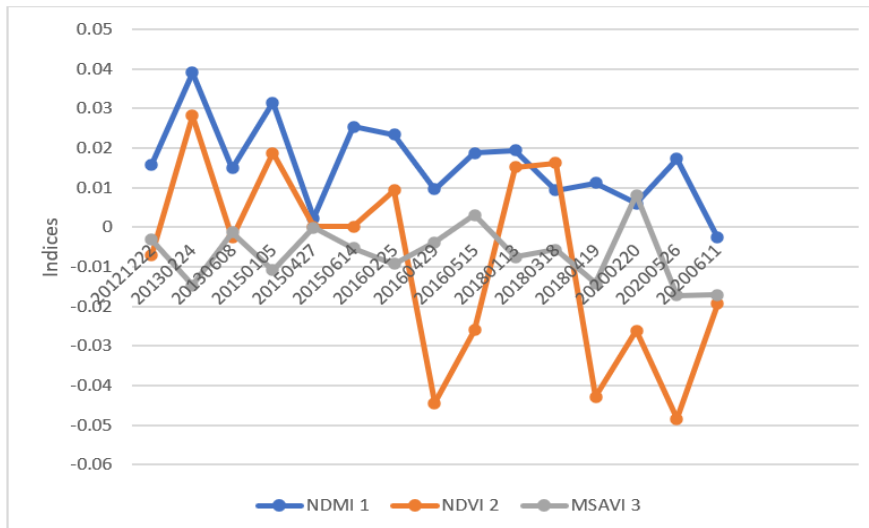
Figure 9. Difference between mean and median values of Spectral Indices

The results from the comparison of the standard deviation of indices in Figure 10. for each flood event showed that apart from 2013, the NDMI standard deviation was low during floods and high before and after flood events. Statistically, a smaller standard deviation implies that the distribution of indices is clustered around the mean, while high standard deviations mean that the data is more spread out. A similar trend was noted in standard deviations of MSAVI and NDVI but with different noise years in 2016 and 2020 where a slight rise in standard deviation was recorded during floods.
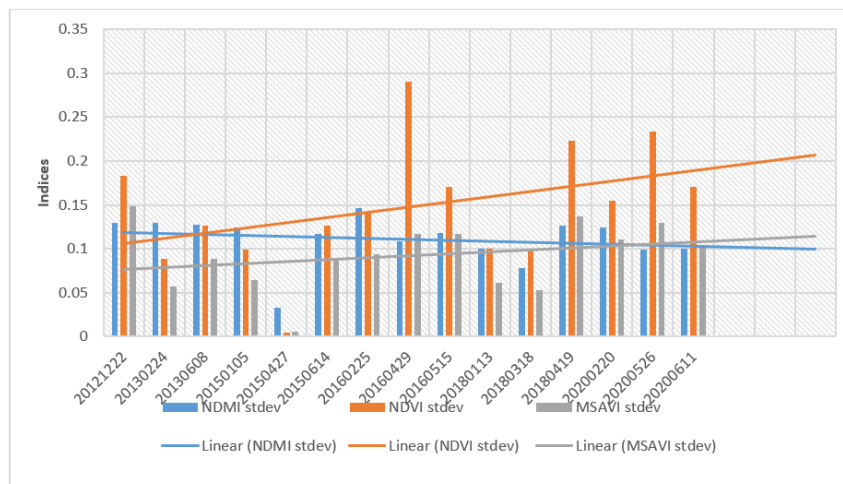

Figure 10. Trend in standard deviation

4.2. Terrain analysis using DEM

Figures 11. and 12. show the DEM of the entire Nairobi County, and the DEM of the Kasarani constituency respectively. The DEM was used to generate the slope and river network characteristics. From the DEM, the elevation of the study area varies from 1455 to 1633 meters above sea level. The lowest elevation was associated with the eastern plains of the Kasarani sub-county and the high elevation values were related to the western part of Nairobi County where most rivers originate.
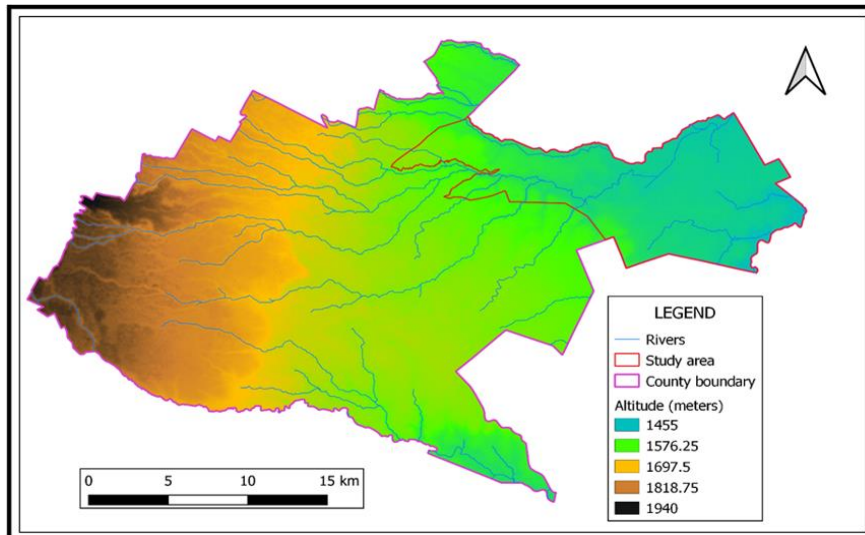
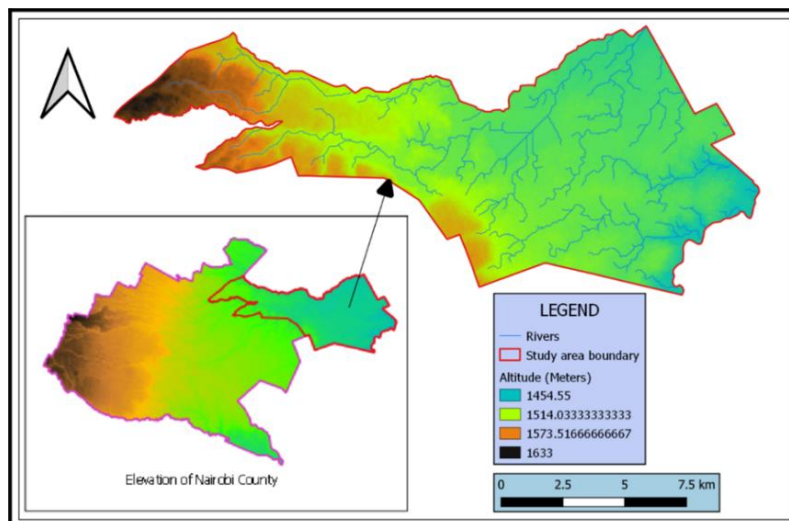**Figure 11**. Digital Elevation Model of Nairobi County

Figure 12: Digital elevation model of Kasarani constituency

5. DISCUSSION

This study sought to examine the degree of the surface on three fronts namely before, during, and after floods, in the area of study, that is Kasarani constituency. The changes were evaluated through the lenses of surging constructions which in turn contribute to upcoming expansive areas of paved surfaces that lower water infiltration and accelerate surface runoff. The NDVI, MSAVI, and NDMI indices were computed to underscore the response of vegetation to floodwater caused by LULC change. Results from a thorough analysis of the floods in the Kasarani constituency in 2013, 2015, 2016, 2018, and 2020 are summarized here.

To begin with, starting from 2013 to 2020, NDVI's mean median and standard deviation values were somewhat higher than those of MSAVI. But, across the flood periods, NDVI and MSAVI showed a common trend. The difference in the values of MSAVI and NDVI can be accounted for by MSAVI's ability to distinguish vegetation from background characteristics (Olmos-Trujillo et al., 2020). Sand particles, traces of clay, and intercalated layers of non-porphyritic basalt rocks form the main background characteristics of the study area (Mwathi, 2016), and paved surfaces from infrastructural development (Mundia, 2017). Consequently, the discrimination of radiations from the background characteristics could have been the cause of low MSAVI values compared to the NDVI.

Secondly, after assessing the Kasarani constituency's NDVI and MSAVI values from 2013 to 2020, while excluding flood days, the mean NDVI stood at between 0.2778 and 0.5406 while that of MSAVI was 0.0642 to 0.3028, a clear indication that there was some substantial vegetation in those environs. Conversely, an evaluation of the area's vegetation led to the observation that showed a decline in NDVI and MSAVI during flood days, which is well documented in Figure 13. by a wave shape graph. The troughs represent the flood days while the crests represent the non-flood days. Paved surfaces are believed to be the cause of the continuous decline in the value of indices seen on flood days. Paved surfaces minimize the ground's porosity and consequently cause floods in the study area. According to Oyugi et al. (2017), the paved surfaces are a result of human activity triggered by urbanization such as the construction of buildings, by-passes, and increased settlement in the Eastern parts of Nairobi such as along Kangundo road, Mwiki, Ruai, and Kamulu.
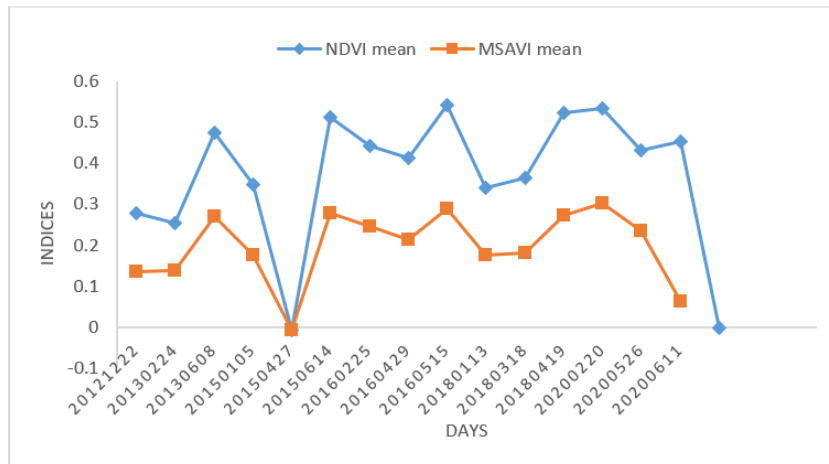
Figure 13. The trend in NDVI and MSAVI mean values

Thirdly, the highest reduction in NDVI and MSAVI indices was observed in the floods of 2015 and 2020. Specifically, the mean value of NDVI during the floods of 2015 declined by 0.35432, while in the 2020 floods, a decline of 0.517 was observed. Also, MSAVI mean values recorded a sharp decline of 0.18243 and 0.0681 during the flood days of 2015 and 2020 respectively. But a drastic reduction in mean values is indicative of a phenological change in LULC which closely relates to the completion of the Eastern by-pass. Per Mundia's (2017) school of thought, the development of towns in Nairobi County occurs along completed corridors, as well as nodes commencing from the CBD. Thus, it's worth noting that the completion of the by-pass construction in 2014 attracted urban sprawl in the study area which resulted in the expansion of areas with impervious surfaces. In 2017, the government of Kenya crafted a roadmap to construct a dual carriageway on the Eastern by-pass to ease auto traffic congestion towards the east of Nairobi County. The vehicles play a crucial role in transporting residents from the Kasarani constituency to the CBD and vice versa. The dualling of the Eastern bypass from 2019 accounts for the decline in MSAVI and NDVI indices observed in 2020.

Fourthly, in the course of the study, the mean values of both NDVI and MSAVI indices rose sharply after every flood event. That rapid rise can be accounted for by the retreat in floodwater in which the vegetation in the study area had been submerged. According to Wanyama et al. (2020) settling of floodwater triggers the sensitivity of vegetation. Consequently, there are high values of infrared but low values of red radiations, which in turn propel a rise in resulting values of vegetation indices.

Fifthly, the majority of flood days saw a rise in the value of NDMI, and this was also seen in the floods of 2015. During that time the lower value before, high value during, and low values after the floods stood at -0.0891, 0.5116, and 0.0722 respectively. A rise in NDMI indices may have resulted from the flood water that led to water-logged conditions on the surface. Besides, it is fundamentally essential to note that most of the water-logged conditions are created by anthropogenic activities such as building and road constructions (Li, 2012) which change the hydrological characteristics of the surface. The rise in NDMI values during floods and reduction during flood-free days marries findings of a study conducted by Sahu and Bengal (2018), which found that water-logged areas recorded higher values of NDMI than areas that had low soil moisture.

Sixthly, in the course of the study, most of the flood days recorded low standard deviation values of NDMI, NDVI, and MSAVI on flood days but those values rose before and after flood events. Statistically, a smaller standard deviation is indicative of a clustered distribution of around the mean but high standard deviations reflect a more spread out. That means the low standard deviations recorded on flood days were indicative of the fact that floodwater had an almost similar effect on the surface reflectance characteristics. Besides, it also meant that floodwater distribution was almost equal in most parts of the Kasarani constituency. Additionally, the equal spread is a result of watertight surfaces resulting from constructions across the area and the flat terrain of the area.

Finally, the Kasarani constituency's terrain lies between 1455 and 1633 meters above sea level, which is a low-lying area when compared to the rest of Nairobi whose sea-level values are between 1455 meters and 1940 meters above sea level. Further, river channels flowing through the area grew following the high Strahler orders of 6 and 4 for Nairobi County and Kasarani constituency respectively. The orders directed that all the main rivers starting from the western part of Nairobi County should flow Eastwards through the plains of the Kasarani constituency. Therefore, the flow of some of Nairobi's main rivers like the Nairobi River, Ngong River, and Pangani River through a low-lying Kasarani constituency aggravate the flooding menace by adding more water to the study area when they break their banks. As a result, environs in the Kasarani constituency that lie along streamlines as well as the extremely low-lying areas in the eastern part of the Kasarani constituency are high-risk flood areas. This is in line with the work of Acha and Aishetu, (2018) who found out that low-lying areas especially along river Benue in Mukurdi flood plains are high flood risk areas. Consequently, the increasing populations that settle along stream networks are more exposed to flooding.

In this study, GIS and remote sensing techniques were utilized to observe the status of the surface before, during, and after flood incidence and the terrain characteristics of the study area. Considering the coherent trend in the response of

vegetation to flood and non-flood days, which reflects the LULC change and topography of the area, it is apparent that frequent floods will continue to intensify with time. The study, therefore, recommends the need to utilize GIS and remote sensing techniques to identify stream channels and water-logged areas which should then be avoided during settlement to reduce vulnerability to floods. Government should also enforce regulations that prohibit settlement along stream channels and review land subdivision policies. Also, all stakeholders such as local communities, non-Governmental organizations, faith-based organizations, and schools' management should frequently be updated on safe evacuation areas as a flood response strategy. Identification of the safe places which generally should be raised and have low soil moisture should be identified using GIS technology.

CONCLUSION AND RECOMMENDATIONS

Kasarani constituency is one of the 17 constituencies in Nairobi County that is mostly exposed to frequent floods. From the EM-DAT report, out of 6 flood incidences that occurred in Kenya between 2010 and 2020, 5 occurred in the area causing effects such as damage to property and displacement of people. This study attempted to assess the status of the surface before, during, and after floods in the Kasarani constituency while relating it to the changes in LULC which could be the cause of intensifying floods. GIS and Remote sensing techniques were utilized in the analysis. Landsat data before, during, and after floods were used to generate the mean, median, and standard deviation of NDVI, MSAVI, and NDMI indices. In addition, SRTM DEM was used in terrain analysis. Changes in the Spectral indices before, during, and after floods were observed and conclusions were drawn from them. Particularly, between a scale of -1 and +1, low values of NDVI and MSAVI indicated flooding while high values indicated retreat of floodwater. In the case of NDMI, on a scale of -1 to +1, high values indicated flooding while low values indicated floodwater retreat. The study area DEM was used to determine low and high-altitude areas, and stream channel generation.

The results revealed that the Kasarani constituency has a substantive amount of vegetation indicated by an NDVI range of between 0.2778 and 0.5406 while the MSAVI range was 0.0642 to 0.3028 on flood-free days. However, the results of the analysis of this area with substantial vegetation showed that the mean values of NDVI and MSAVI declined during flood days. NDMI values recorded an increase in value during flood days and a decrease on flood-free days. The results of DEM analysis indicated that the elevation of the study area varies from 1455 to 1633 meters above sea level. When compared to the elevation of the entire Nairobi County which ranges between 1455 meters and 1940 meters, the Kasarani constituency was observed to be a low-lying area with all stream channels of Nairobi County traversing it. This study, therefore, illustrates a coherent and low-cost technique for detecting the status of the surface before, during, and after flood incidences. Identifying the status of the surface is a key step in flood management as it helps to guide planners and policymakers in legislating policies that foster sustainable urban development. Also, the study can be used by stakeholders such as local communities, non-governmental organizations, Faith-based organizations, and schools' management in flood response by identifying safe areas for the evacuation process.

References

[1]. Abuya, D. O. (2020). *Management Of The Effects Of Land Use Changes On Urban Infrastructure Capacity: A Case Study Of Ruaka Town, Kiambu County, Kenya* (Doctoral dissertation, University of Nairobi).

[2]. Acha, S. and Aishetu, A. (2018). Spatio-temporal changes of land use land cover dynamics and its implication on urban flood vulnerability in Makurdi, Nigeria. *Journal of Research in Forestry, Wildlife and Environment*, *10*(2), 65-69.

[3]. Aljahdali, M. O., Munawar, S., and Khan, W. R. (2021). Monitoring mangrove forest degradation and regeneration: Landsat time series analysis of moisture and vegetation indices at Rabigh Lagoon, Red Sea. *Forests*, *12*(1), 52.

[4]. Barnsley, M. J., and Barr, S. L. (2000). Monitoring urban land use by earth observation. *Surveys in Geophysics*, *21*(2), 269-289.

[5]. Brody, S. D., Highfield, W. E., and Kang, J. E. (2011). *Rising waters: The causes and consequences of flooding in the United States*. Cambridge University Press.

[6]. Cui, X.; Gibbes, C.; Southworth, J.; Waylen, P.; Cui, X.; Gibbes, C.; Southworth, J.; Waylen, P.(2013). Using Remote Sensing to Quantify Vegetation Change and Ecological Resilience in a Semi-Arid System. *Land,* 2(1), 108–130

[7]. Dammalage, T. L., and Jayasinghe, N. T. (2019). Land-use change and its impact on urban flooding: A case study on Colombo district flood on May 2016. *Engineering, Technology & Applied Science Research*, 9(2), 3887-3891.

[8]. Dewan, A. M., and Yamaguchi, Y. (2009). Land use and land cover change in Greater Dhaka, Bangladesh: Using remote sensing to promote sustainable urbanization. *Applied geography*, *29*(3), 390-401.

[9]. Dwyer, J. L., Roy, D. P., Sauer, B., Jenkerson, C. B., Zhang, H. K., and Lymburner, L.(2018). Analysis ready data: enabling analysis of the Landsat archive. *Remote Sensing*, *10*(9), 1363.

[10]. Ejikeme, J., Igbokwe, J., Igbokwe, E., and Paul, C. (2020). Application of Knowledge-Based Image Classification and Ca-Markov Chain Prediction Model for Landuse/Landcover Change Analysis of Onitsha and Environs, Anambra State. *Int. J. Adv. Res. Publ*, *4*(1), 22-28.

[11]. Emmett, K. D., Renwick, K. M., and Poulter, B. (2019). Disentangling climate and disturbance effects on regional vegetation greening trends. *Ecosystems*, *22*(4), 873-891.

[12]. Guzha, A. C., Rufino, M. C., Okoth, S., Jacobs, S., and Nóbrega, R. L. B. (2018). Impacts of land use and land cover change on surface runoff, discharge and low flows: Evidence from East Africa. *Journal of Hydrology: Regional Studies*, *15(1), 49-67.*

[13]. Hemati, M., Hasanlou, M., Mahdianpari, M., and Mohammadimanesh, F. (2021). A systematic review of landsat data for change detection applications: 50 years of monitoring the earth. *Remote Sensing*, *13*(15), 1-33.

[14]. Hussein, K., Alkaabi, K., Ghebreyesus, D., Liaqat, M. U., and Sharif, H. O. (2020). Land use/land cover change along the Eastern Coast of the UAE and its impact on flooding risk. *Geomatics, Natural Hazards and Risk*, 11(1), 112-130.

[15]. Idowu, D., and Zhou, W. (2021). Land Use and Land Cover Change Assessment in the Context of Flood Hazard in Lagos State, Nigeria. *Water*, *13*(8), 1-17.

[16]. KNBS. (2019). 2019 Kenya Population and Housing Census. Nairobi.

[17]. Lauer, D. T., Morain, S. A., and Salomonson, V. V. (1997). The Landsat program: Its origins, evolution, and impacts. *Photogrammetric Engineering and Remote Sensing*, *63*(7),831- 838.

[18]. Lee, Y., and Brody, S. D. (2018). Examining the impact of land use on flood losses in Seoul, Korea. *Land use policy*, *70*, 500-509.

[19]. Li, C. (2012). Ecohydrology and good urban design for urban storm water-logging in Beijing, China. *Ecohydrology and Hydrobiology*, *12*(4), 287-300.

[20]. Li, C., Liu, M., Hu, Y., Shi, T., Qu, X., and Walter, M. T. (2018). Effects of urbanization on direct runoff characteristics in urban functional zones. *Science of the Total Environment*, 643(1), 301-311.

[21]. Li, G., Wang, J., Wang, Y., Wei, H., Ochir, A., Davaasuren, D., and Nasanbat, E. (2019). Spatial and temporal variations in grassland production from 2006 to 2015 in Mongolia along the China–Mongolia railway. *Sustainability*, *11*(7), 2177.

[22]. Lulla, K., Nellis, M. D., Rundquist, B., Srivastava, P. K., and Szabo, S. (2021). Mission to earth: LANDSAT 9 will continue to view the world. *Geocarto International*, *36*(20), 2261-2263.

[23]. Masese, A., Neyole, E., and Ombachi, N. (2016). Loss and Damage from Flooding in Lower Nyando Basin, Kisumu County, Kenya. *International Journal of Social Science and Humanities Research*, *4*(3), 9-22.

[24]. Mishra, N. B., and Mainali, K. P. (2017). Greening and browning of the Himalaya: Spatial patterns and the role of climatic change and human drivers. *Science of the Total Environment*, *587*, 326-339.

[25]. Muema, R., and Officer, C. (2016). *Nairobi City County Development Plans and Policies*. Nairobi: Kenya Property Developers Association.

[26]. Mundia, C. N. (2017). Nairobi metropolitan area. In Urban development in Asia and Africa (pp.293-317). Springer, Singapore.

[27]. Mundia, C. N., and Aniya, M. (2006). Dynamics of land use/cover changes and degradation of Nairobi City, Kenya. *Land Degradation & Development*, *17*(1), 97-108.

[28]. Muthusi,N.N.; Dulo,S.O. and Ndiba, P. K.(2020) Runoff Estimation for an Urban Area using SCS-CN Method, Remote Sensing and Geographic Information Systems Approach: A Case Study of Mavoko Municipality, Kenya.International Journal of Engineering Research & Technology,9(4), 854-859.

[29]. Mwathi, P. M. (2016). *Effects of land use and land cover dynamics on environmental quality of Nairobi city and its environs* (Doctoral dissertation, University of Nairobi).

[30]. Okaka, F. O., and Odhiambo, B. (2018). Relationship between flooding and outbreak of infectious diseases in Kenya: a review of the literature. *Journal of environmental and public health*, *2018*(1),1-8.

[31]. Okoola, R. E. (1996). *Space-time characteristics of the ITCZ over equatorial Eastern Africa during anomalous rainfall years*. Nairobi: University of Nairobi.

[32]. Olmos-Trujillo, E., González-Trinidad, J., Júnez-Ferreira, H., Pacheco-Guerrero, A., Bautista-Capetillo, C., Avila-Sandoval, C., and Galván-Tejada, E. (2020). Spatio- temporal response of vegetation indices to rainfall and temperature in a semiarid region. Sustainability, 12(5), 1939.

[33]. Oyugi, M. O., Odenyo, V. A., and Karanja, F. N. (2017). The implications of land use and land cover dynamics on the environmental quality of Nairobi City, Kenya. *American Journal of Geographic Information System*, *6*(3), 111-127.

[34]. Qi, J., Chehbouni, A., Huete, A. R., Kerr, Y. H., and Sorooshian, S. (1994). A modified soil adjusted vegetation index. *Remote sensing of environment*, *48*(2), 119-126.

[35]. Sahu, A. S., and Bengal, N. W. (2018). Detection of water-logged areas using geoinformatics techniques and relationship study in Panskura-Tamluk flood plain (India). *Trans. Inst. Indian Geographers*, *40*(1), 9-24.

[36]. Sakai, T., Hatta, S., Okumura, M., Hiyama, T., Yamaguchi, Y., and Inoue, G. (2015). Use of Landsat TM/ETM+ to monitor the spatial and temporal extent of spring breakup floods in the Lena River, Siberia. *International Journal of Remote Sensing*, *36*(3), 719-733.

[37]. Tucker, C. J. (1979). Red and photographic infrared linear combinations for monitoring vegetation. *Remote sensing of Environment*, *8*(2), 127-150.

[38]. Vermote, E., Justice, C., Claverie, M., and Franch, B. (2016). Preliminary analysis of the performance of the Landsat 8/OLI land surface reflectance product. *Remote Sensing of Environment*, *185*, 46-56.

[39]. Wanyama, D., Moore, N. J., and Dahlin, K. M. (2020). Persistent vegetation greening and browning trends related to natural and human activities in the Mount Elgon ecosystem. *Remote Sensing*, *12*(13), 2113.

[40]. Wulder, M. A., Loveland, T. R., Roy, D. P., Crawford, C. J., Masek, J. G., Woodcock, C. E., and Zhu, Z. (2019). Current status of Landsat program, science, and applications. *Remote sensing of environment*, 225(1), 127-147.

[41]. Zhu, Z., Wulder, M. A., Roy, D. P., Woodcock, C. E., Hansen, M. C., Radeloff, V. C., ... & Scambos, T. A. (2019). Benefits of the free and open Landsat data policy. *Remote Sensing of Environment*, 224(1), 382-385.

[42]. Zope, P. E., Eldho, T. I., and Jothiprakash, V. (2015). Impacts of urbanization on flooding of a coastal urban catchment: a case study of Mumbai City, India. *Natural Hazards*, *75*(1), 887-908.

[43]. Zope, P. E., Eldho, T. I., and Jothiprakash, V. (2016). Impacts of land use–land cover change and urbanization on flooding: A case study of Oshiwara River Basin in Mumbai, India. *Catena*, *145*, 142-154.

INTERNET SOURCES

Internet 1. https://www.usgs.gov/landsat-missions/landsat-collection-2-level-2-science-products.

Internet 2. https://www.standardmedia.co.ke/business/real-estate/article/2000203048/.

Internet 3. https://espa.cr.usgs.gov/.

Internet 4. https://gadm.org.

Internet 5. https://en.climate-data.org/.